J Mater Sci (2007) 42:2290–2296
DOI 10.1007/s10853-006-0615-5

Studies on electrodeposition of corrosion resistant Ni–Fe–Mo alloy

Renato A. C. Santana · Shiva Prasad · Elisangela S. Moura · Ana R. N. Campos · Gecilio P. Silva · Pedro Lima-Neto

Received: 4 November 2005 / Accepted: 22 June 2006 / Published online: 27 February 2007

Abstract A study to optimize the process parameters for electrodeposition of a Ni–Fe–Mo alloy is reported. A 2^2full factorial design was successfully employed for the experimental design analysis of the results. The optimum experimental conditions for producing the corrosion resistant alloy were 120 mA/cm^2 current density, 20 rpm cathode rotation, 9.0 pH at 30 °C. The alloy was deposited at 61% current efficiency, with an average composition of 62 wt% Ni, 17wt% Fe, 21wt% Mo and traces of boron, and with E_{corr} –0.506 V, R_p 8.883×10^3 Ohm cm^2 and I_{corr} 6.468×10^{-7} A/cm^2. The deposit obtained under these conditions had an amorphous character, good adherence, high corrosion resistance and a nodular morphology. Electrochemical corrosion tests verified that the electrodeposited Ni–Fe–Mo alloy had better corrosion resistance than the Fe–Mo alloy.

Introduction

Molybdenum alloys are of interest due to their desirable properties, such as a high corrosion resistance, high wear resistance [1] and low hydrogen evolution overpotential [2, 3]. These alloys may also act as catalysts for hydroprocessing of aromatic oils and gas phase hydrogenation of benzene. Molybdenum alloys can be produced by electrodeposition [4]. From a theoretical point of view, electrodeposition of these alloys is an example of the induced codeposition mechanism [5]. In spite of numerous claims, the electrodeposition of molybdenum in the pure state from aqueous solutions has been unsuccessful. However, electrolytic induced codeposition of molybdenum occurs with iron-group metals [6]. Several authors have investigated the process of electrodeposition of tungsten with iron group metals in aqueous solutions [7–10].

Conventional and classical methods of studying a process by maintaining other factors involved at an unspecified constant level does not allow for assessments of the combined effects of several or all of the factors involved. This method is also time consuming and requires large number of experiments to define optimized levels, with respect to individual parameters. However, these optimization procedures are often unreliable for assessing the optimized combined performance. These limitations of a conventional method can be eliminated by optimizing all of the control variables parameters collectively and simultaneously through the use of statistical experimental design such as Response Surface Methodology (RSM) [11]. Experimental factorial design investigations present several advantages over univariant methods. The control variables (factors) are varied simultaneously rather than one-at-a-time, so that it is possible to observe the synergistic and antagonistic interactions among the factors. Univariant methods are incapable of measuring these interactions, and, therefore, are not effective optimization techniques. RSM is a collection of mathematical and statistical techniques that are useful for developing, improving

R. A. C. Santana · S. Prasad (✉) · E. S. Moura · A. R. N. Campos · G. P. Silva · P. Lima-Neto
Department of Chemical Engeering, Universidade Federal de Campina Grande, Post Box 10108, Campina Grande, Paraiba 58109-970, Brazil
e-mail: prasad@deq.ufcg.edu.br

and optimizing processes; RMS can be used to evaluate the relative significance of several affecting factors even in the presence of complex interactions. The main objective of RSM is to determine the optimum operational conditions for the system or to determine the regime of control variables that satisfies the operating specifications [12].

The results of a study to optimize the operational conditions (current density, bath temperature) for the electrodeposition of an Ni–Fe–Mo alloy is reported here. The interaction between the parameters was evaluated and optimized using response surface methodology.

Experimental

Bath composition and substrate

The electrochemical bath was prepared using analytical grade chemicals and double distilled, deionized water. The bath used for electrodeposition of the Ni–Fe–Mo alloy contained 0.03 M nickel sulfate, 0.010 M iron sulfate, 0.028 M sodium molybdate, 0.0728 M boron phosphate, 0.0323 M sodium citrate and 0.017 g/L 1-Na-dodecylsulfate. The bath pH was adjusted initially and during the deposition process using either ammonium hydroxide or sulfuric acid. Ammonium hydroxide is preferred to NaOH for pH adjustment since it stabilizes the bath by its complexing action. The electrodeposition process was usually performed for a period of 1 h.

Prior to the coating deposition, the substrate was polished to 1200 grit surface finish. The electrodeposition was performed under galvanostatic control on a rotating rectangular copper foil cathode with a surface area of approximately 8 cm^2, which was placed inside a cylindrical platinum gauze anode. All specimens were subjected to a series of cleaning steps with a final rinse in dilute 10% H_2SO_4 to remove any residual alkali [13].

Electrodeposition

A potentiostat/galvanostat (Autolab PGSTATE 30) was used to apply a known current density to the cathode. An MTA KUTESZ MD2 thermostat controlled the temperature of the bath and a rotating electrode, EG&G PARC 616 (cathode rotation), was used to control mechanical agitation. The Faradaic efficiency was calculated from the charge passed and the equivalent weight gained. The alloy composition was taken into account when calculating the deposition efficiency.

Table 1 Actual and coded levels of factors studied

Factors	Code		
	–1	0	+1
Current Density/mA/cm^2	60	90	120
Temperature/°C	30	50	70

Response surface methodology

RSM was used to design this experiment. A complete factorial design of two levels and two factors (2^2) was used [14], with three replicates at the centre point. Thus, a total 7 experiments were employed in this study for a quantitative evaluation of the influence of current density and bath temperature on the alloy deposition efficiency and corrosion resistance (polarization resistance). Table 1 lists the levels of the factors used, as well as their experimental design codes. Each independent factor was investigated at a high (+1) and a low (–1) level. The centre point (0) replicates were chosen to verify any change in the estimation procedure, as a measure of precision property. For statistical calculations, coding of the independent variables was done according to the following Equation:

$$x_i = \frac{(X_i - X_o)}{\Delta X_i} \tag{1}$$

where x_i and X_i are the dimensionless and the actual values of the independent variable i, X_o the actual value of the independent variable i at the central point, and ΔX_i the step change of X_i corresponding to a unit variation of the dimensionless value.

The behaviour of the system was explained by the following linear Equation

$$Y = \beta_o + \beta_1 x_1 + \beta_2 x_2 + \beta_{12} x_1 x_2 \tag{2}$$

The coefficients of the polynomial were represented by β_0 (constant term), β_1 and β_2 (linear effects), and β_{12} (interaction effects). The analysis of variance (ANOVA) tables were generated, and the effect and regression coefficients of individual linear and interaction terms were determined. The significances of all terms in the linear relationship were judged statistically by computing the F-value at a probability (P) of < 0.05.

The objective of using RSM is not only to investigate the response over the entire factor space, but also to locate the region of interest where the response

reaches its optimum or near optimal value. By carefully studying the response surface model, the combination of factors that gives the best response can then be established [15].

The results of the experimental design were studied and interpreted by MATLAB 6.5 software to estimate the response of the dependent variable.

Corrosion resistance

The potentiodynamic linear polarization (PLP) and electrochemical impedance spectroscopy (EIS) studies were performed using a potentiostat (Autolab PGSTATE 30) for corrosion analysis. A saturated calomel electrode (Hg/Hg_2Cl_2) and Pt foil were used as reference and auxiliary electrodes, respectively. The PLP curves were obtained with a sweep rate of 0.001 V/s in a potential range –1.0 V to 2.0 V. The impedance experiments were carried out at specific potentials selected from the PLP curves with a frequency interval of 100 kHz to 0.004 Hz and at 0.01 V amplitude. The specimens were stabilized for a period of 1 hour prior to initiating the PLP and EIS tests. All of the electrochemical corrosion tests were conducted in aqueous 1 M NaCl at room temperature and in ambient atmosphere.

Characterization of the deposit

Characterization of the structure of the alloy was determined by X-ray diffraction (XRD), using a Siemens D500 Diffractometer, with Cu Kα radiation, a step size of 0.02° and a dwell time of 1s.

The surface morphology and the cross-section microstructure of the electrodeposited layers were characterized by scanning electron microscopy (SEM) using a Philips XL-30 scanning electron microscope. The approximate composition of the alloy was determined by energy dispersive X-ray analysis (EDX) using a Link Analytical QX-2000 attached to the SEM apparatus. Presence of boron in the alloy was determined by atomic absorption spectrometric analysis.

Results and discussion

All the seven electrodeposition experiments were conducted in duplicate and the average values of electrodeposition efficiency and corrosion resistance (corrosion potential) along with design matrix are tabulated in Table 2. As part of the data analysis, the goodness of fit of the model is required. The evaluation of the model adequacy includes a test for significance of the regression model, a test for the significance of the model coefficients, and a test for lack of fit. For this purpose, analysis of variance (ANOVA) was performed.

The results were subjected to multiple non-linear regression analysis to obtain coefficients for each of the parameters. Estimates of the coefficients with levels higher than 95% ($P < 0.05$) were included in the final model. Deposition efficiency (*Eff.*) and polarization resistance (R_p), can thus be expressed as functions of the independent factors by the linear mathematical model represented by Eqs. 3 and 4 respectively, where (I) is current density, and (t) is temperature. Taking into account only the significant effects, the following equations correspond to the surface response shown in Figs. 1 and 2.

$$Eff.(\%) = 71.25 - 2.95I + 4.48t + 0.93I * t \quad (3)$$

$$R_p = 3638.37 + 1373.60I - 2832.60t - 729.40I * t \quad (4)$$

The value R^2 obtained was equal to 99% and 97% for *Eff.* and R_p, respectively. This means that the regression model provides an excellent explanation of the relationship between the independent variables (factors) and the response (*Eff.* and R_p). The associated P-value for the model is lower than 0.05 (i.e. $\alpha = 0.05$, or 95% confidence), which indicates that the model is considered statistically significant. The variance and regression analyses demonstrated the statistical significance of the models, justifying the use of a linear model for the statistical analysis. The statistical significance of the ratio of the mean square variation due to regression and

Table 2 Electrodeposition efficiency, corrosion resistance and deposit composition as shown by the factorial matrix

Runs	Current density	Temp. (°C)	R_p/Ohm cm^2	I_{corr}/A/cm^2	E_{corr}/V	Deposition efficiency/%
1	–1	–1	4677	6.07×10^{-6}	–0.767	70.501
2	–1	+1	470.6	5.93×10^{-5}	–0.851	77.598
3	+1	–1	8883	6.47×10^{-7}	–0.506	62.727
4	+1	+1	1759	2.78×10^{-5}	–0.800	73.543
5	0	0	2934	2.71×10^{-5}	–0.792	72.123
6	0	0	3237	2.99×10^{-5}	–0.791	73.813
7	0	0	3508	2.11×10^{-5}	–0.775	73.451

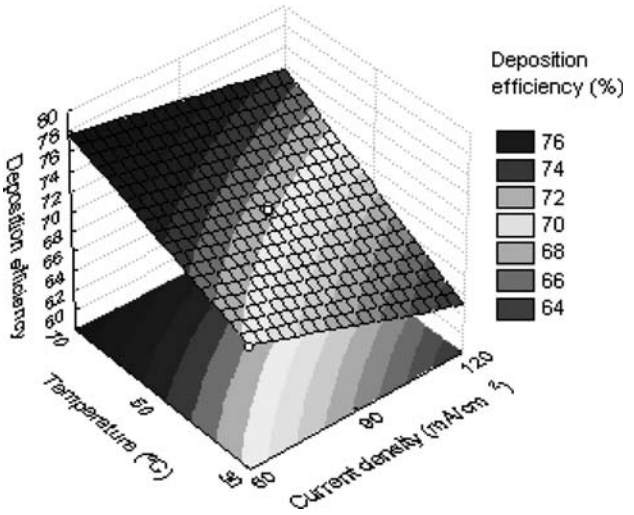

Fig. 1 Fitted surface of influence of current density vs. temperature in relation to deposition efficiency of the alloy, using a bath pH of 9.0 and rotation rate at 20 rpm

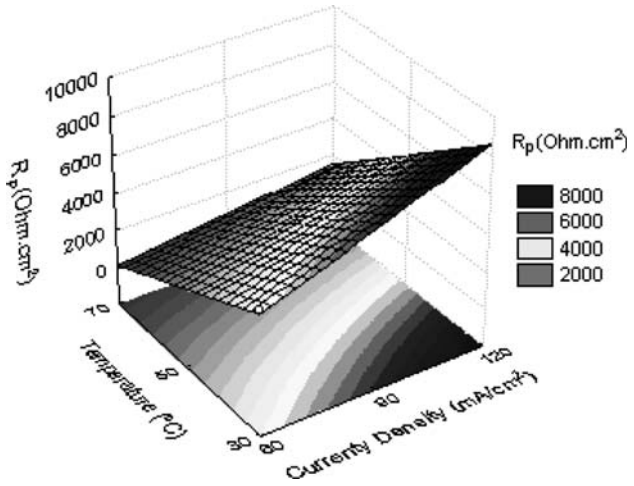

Fig. 2 Fitted surface of influence of current density vs. temperature in relation to polarization resistance of the alloy, using a bath pH of 9.0 and rotation rate at 20 rpm

mean square residual error was tested using the analysis of variance (ANOVA) [16]. ANOVA is a statistical technique that subdivides the total variation in a set of data into component parts associated with specific sources of variation for the purpose of testing hypotheses on the parameters of the model. According to the ANOVA (Tables 3, 4), the F values for all regressions were large. The large value of F indicates that most of the variation in the response can be explained by the regression equation. A P value lower than 0.05 indicates that the model is considered to be statistically significant [17]. The P values for all of the regressions were lower than 0.05. This means that at least one of the terms in the regression equation has a significant correlation with the response variable.

Effect of current density

The effect of current density on process efficiency was studied in the range 60–120 mA/cm^2. The highest value for the deposition efficiency, approximately 77%, was obtained by using the lower current density of 60 mA/cm^2. From the experimental data (Table 2) it was observed that a decrease in current density and an increase in temperature (Equation 3) increased deposition efficiency (Fig. 1). Similar behaviour was observed by Weikang et al. [18]. This should be associated with a higher deposition of nickel at lower current density 60 mA/cm^2 [18]. From Equation 4 it is observed that the current density was one of the factors that influenced corrosion resistance of the deposit. It was observed that an increase in current density and a decrease in temperature increased corrosion resistance (Fig. 2). The best results for corrosion resistance (i.e. polarization resistance) were obtained with a current density 120 mA/cm^2. Similar results were demonstrated by corrosion current density measurements as showed in Table 2. High current densities favour the deposition of Mo, as reported by Brenner et al. [19] who observed a significant increase in Mo content with increasing current density in citrate bath.

Effect of temperature

Temperature is another important factor in the operation of molybdenum alloy plating baths. An increase

Table 3 Results of ANOVA of deposit efficiency

Source	Sum of squares	Degrees of freedom	Mean square	F	P
(1) Current density	34.981	1	34.981	221.852	0.000
(2) Temperature	80.218	1	80.218	508.751	0.000
Interaction 1 and 2	3.457	1	3.457	21.929	0.018
Residual error	0.473	3			
Lack of fit	0.234	1			
Pure error	0.238	2			
Total	119.601	6			

Table 4 Results of ANOVA of corrosion resistance (R_p)

Source	Sum of squares	Degrees of freedom	Mean square	*F*	*P*
(1) Current density	7547108	1	7547108	21,43599	0,018977
(2) Temperature	32094491	1	32094491	91.15772	0.002437
Interaction 1 and 2	2128097	1	2128097	6.04442	0.090986
Residual error	1056229	3	352076		
Lack of fit	891321	1	891321		
Pure error	164909	2	82454		
Total	42825926	6			

in temperature usually decreases polarization, increases the concentration of metal in the cathode diffusion layer, and may affect the cathode current efficiency for metal deposition, particularly those deposited from complex ions. The effect of bath temperature on the process efficiency was studied in the temperature range 30–70 °C. From Table 3, it can be confirmed that the temperature change had the most statistically significant effect on the process efficiency at the 95% level.

The statistical results obtained in this study suggest that the increase in the bath temperature increases the deposition efficiency. The best results (good quality deposits) were obtained at 70 °C with a deposition efficiency of 77%. Figure 1 shows the estimated response surface for current efficiency in relation to the current density and temperature.

The effect of current density and temperature on corrosion resistance is shown in Fig. 2. Bath temperature showed a statistically significant effect on corrosion resistance of the deposit (Eq. 4, Table 4). The statistical results obtained in this study suggest that the decrease in bath temperature increased corrosion resistance of the deposit.

Appearance of the deposit

From the SEM analysis, it was observed that the Ni–Fe–Mo alloy (Fig. 3) deposited on the copper substrate did not exhibit any microcracks. The SEM micrograph shown in Fig. 3 demonstrates that the surface of the deposit had a coarse nodular structure.

The deposit also showed good adherence and lustre, with an average thickness of 36 μm after 1 h of electrodeposition. The approximate composition of the electrodeposited alloy obtained via energy dispersive x-ray spectroscopy was 62wt% Ni, 17wt% Fe, 21wt% Mo. Atomic absorption spectrometric analysis showed the presence of some (≈1%) boron in all the deposits.

The amorphous character of the as-deposited alloy was confirmed by XRD. Boron was added to the bath in the form of boron phosphate, which was co-deposited with the Ni–Fe–Mo alloy, producing an amorphous structure. According to Einati et al. the addition of boron favours the formation of amorphous structure besides increase in resistance of thin films, improving the stability of these films against the air oxidation [20].

Corrosion resistance

The conditions for depositing a corrosion resistant Ni–Fe–Mo alloy were: current density of 60 mA/cm^2, bath temperature of 30 °C, pH 9.0 and rotation rate at 20 rpm. This gave a deposition efficiency of about 61%. The average composition of the deposit was 62wt% Ni, 17wt% Fe, 21wt% Mo, giving a corrosion potential of –0.506 V and a polarization resistance of 8.883×10^3 Ohm cm^2.

An Fe–Mo alloy was also produced via electrodeposition, and used for comparison with the Ni–Fe–Mo alloy. The Fe–Mo specimen was obtained using a current density of 20 mA/cm^2, at 70 °C, with a pH of 6.0 and rotation rate at 20 rpm which gave a deposition efficiency of about 30%. The average composition of the deposit was 70 wt% Fe, 30 wt% Mo with traces of boron giving a corrosion potential of –0.948 V and a polarization resistance of 1.260×10^3 Ohm cm^2. These results were obtained using the response surface

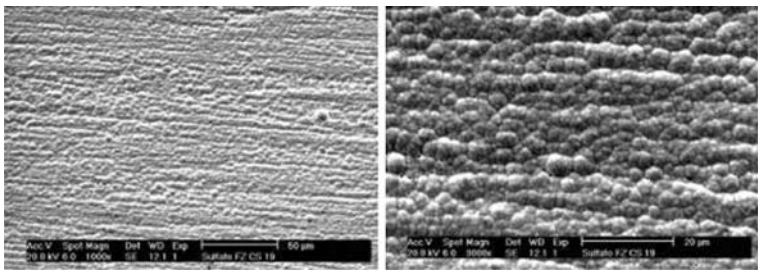

Fig. 3 SEM diagrams of the Ni–Fe–Mo alloy surface with 1000 × and 3000 × amplification (current density 60 mA/cm^2, temperature 30 °C, pH 9.0 and rotation rate 20 rpm)

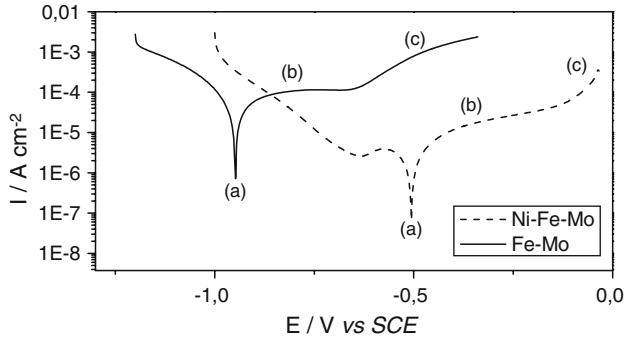

Fig. 4 Anodic polarization curve of the Fe–Mo alloy (current density 20 mA/cm^2, temperature 30 °C, pH 6.0 and rotation rate 20 rpm); and anodic polarization curve of the Ni–Fe–Mo alloy (current density 60 mA/cm^2, temperature 70 °C, pH 9.0 and rotation rate 20 rpm)

Table 5 Corrosion data obtained from potentiodynamic polarization curves

Corrosion data	Ni–Fe–Mo	Fe–Mo
E_{corr}/V	–0.506	–0.948
R_p/Ohm cm^2	8.883×10^3	1.260×10^3

methodology to optimize the effects of the operational parameters in this system.

Corrosion characterization of the alloy Ni–Fe–Mo deposited on copper substrate with the optimized operational parameters was evaluated by linear polarization curves. Potentiodynamic curves obtained for the alloys Fe–Mo and Ni–Fe–Mo deposited under optimal conditions for corrosion resistance in 1 M NaCl are shown in Fig. 4. These curves show that the electrodeposits containing Ni–Fe–Mo had corrosion potentials 442 mV more positive than that of the electrodeposit containing Fe–Mo. The dissolution process was observed for both the alloys, but the deposit Ni–Fe–Mo showed higher resistance to the corrosion process (Table 5).

Electrochemical impedance experiments were performed to obtain detailed information about the corrosion resistance behaviour and to confirm the results obtained by the PLP study of Ni–Fe–Mo and Fe–Mo alloys. The impedance measurements were performed in the regions a-c marked on the polarization curves of Fig. 4.

Figure 5 shows the impedance diagram, which represents the corrosion potential correlated to point (a). Figures 6 and 7 correspond to the potentials represented by (b) and (c), respectively.

The Ni–Fe–Mo alloys had higher impedance values than the Fe–Mo alloy, thus confirming the higher corrosion resistance (R_p) of the former. Additionally, Fig. 6 shows typical diagrams for the process of passivation and dissolution that confirm the findings of the

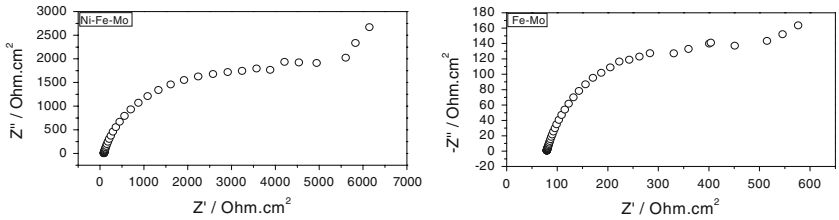

Fig. 5 Impedance diagrams related to the point (a) of the anodic polarization curves of the Ni–Fe–Mo and Fe–Mo alloys

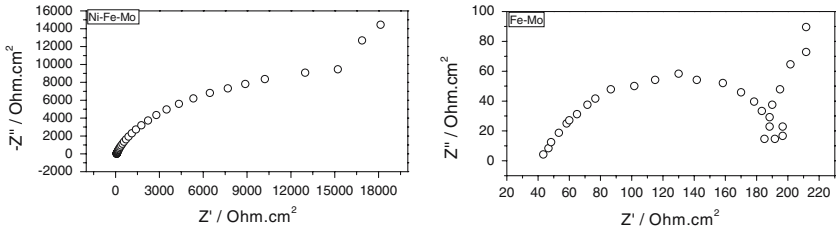

Fig. 6 Impedance diagrams related to the point (b) of the anodic polarization curves of the Ni–Fe–Mo and Fe–Mo alloys

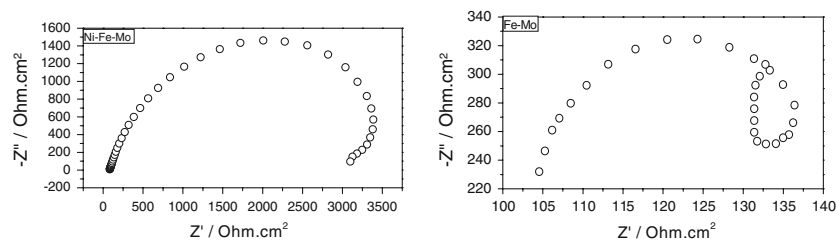

Fig. 7 Impedance diagrams related to the point (c) of the anodic polarization curves of the Ni–Fe–Mo and Fe–Mo alloys

polarization curves, which suggested the presence of an unstable passive film on the surface. The same type of passivation and dissolution process was also observed by Santana et al. [13] and Keddam et al. [21]. Figure 7 shows the impedance diagrams, which are associated with transpassivation and could be attributed to the dissolution process of the passive film as was also observed by Keddam et al. [21–23] and Bojinov et al. [24]. By the end of the impedance tests on the Fe–Mo alloy, almost complete dissolution of the electrodeposited film had occurred, exposing the surface of the copper substrate after about 4 h of total impedance scan time. In the case of the Ni–Fe–Mo alloy film of about the same thickness, which was exposed to the same corrosion medium and for the same period, the copper substrate surface did not become visible.

Conclusions

For the optimized bath composition and within the range of operating parameters evaluated in this study, it has been shown that:

1. For electrodeposition of the Ni–Fe–Mo alloy at an efficiency of 77%, the optimized values of operational parameters were: cathode current density 60 mA/cm^2,bath temperature 70 °C, pH 9.0 and rotation rate at 20 rpm.
2. Good deposits in terms of corrosion resistance were obtained under the following operational conditions: current density 120 mA/cm^2, bath temperature 30 °C, pH 9.0 and rotation rate at 20 rpm giving a deposition efficiency of 61%.
3. The deposits obtained under optimum conditions for both deposition efficiency and corrosion resistance were of an amorphous nature, as evidenced by XRD. These deposits exhibited a nodular morphology, good adherence and lustre.

Acknowledgements The authors are grateful to CNPq, CAPES and FINEP for financial assistance and to PRH-25/ANP/MCT for a fellowship to one of the authors (RACS), to FUNCAP for a scholarship to G. P. da Silva.

References

1. Kinh VO, Chassaing E, Saurat M (1975) Electrodeposition Surf Treat 3:205
2. Crnkovic FC, Machado SAS, Avaca LA (2004) J Hydrogen Energy 29:249
3. Kawashima A, Akiyama E, Habazaki H, Hashimoto K (1998) Mater Sci Eng A 905:226
4. Kriz JF, Shimada H, Yoshimura Y, Matsubayashi N, Nishijima A (1995) Fuel 74:1852
5. Gomez E, Pellicer E, Valles E (2003) J Appl Electrohem 33:245
6. Marinho FA, Santana FSM, Vasconcelos ALS, Santana RAC, Prasad S (2002) J Braz Chem Soc 13:522
7. Podhala EJ, Landolt D (1996) J Electrochem Soc 143:885
8. Donten M, Cesiulis H, Stojek Z (2005) Electrochim Acta 50:1405
9. Sanches LS, Domingues SH, Marino CEB, Mascaro LH (2004) Electrochem Commun 6:543
10. Beltowska-Lehman E (2002) Surf Coat Tech 151:440
11. Murat E (2002) Process Biochem 38:667
12. Annadurai G, Juang RS, Lee DJ (2002) Adv Inorg Environ Res 6:191
13. Santana RAC, Prasad S, Campos ARN, Araújo FO, Da Silva GP, de Lima-Neto P (2006) J Appl Electrochem 36:105
14. Ruotolo LAM, Gubulin JC (2003) J Appl Electrochem 33:1217
15. Ravikumar K, Pakshirajan K, Swaminathan T, Balu K (2005) Chem Eng J 105:131
16. Shashikant VG, Raheman H (2006) Bioresource Technol 97:379
17. Kansal HK, Singh S, Kumar P (2005) J Mater Process Technol 169:427
18. Weikang H, Yunshi Z, Deying S, Zuoxiang Z, Yun W (1995) Mater Chem Phys 41:141
19. Brenner A, Burkhead PS, Seegmiller E (1947) J Res Natl Bur Stand 39:351
20. Einati H, Bogush V, Sverdlov Y, Rosenberg Y, Shacham-Diamand Y (2005) Microelectron Eng 82:623
21. Keddam M, Mattos OR, Takenouti HJ (1981) J Electrochem Soc 128:257
22. Keddam M, Lizee JF, Pallotta C, Takenouti HJ (1984) J Electrochem Soc 131:2016
23. Keddam M, Mattos OR, Takenouti HJ (1986) Electrochim Acta 31:1147
24. Bojinov M, Betova I, Raicheff R (1998) Electrochim Acta 44:721